Analysis of the Rydberg character of the $5d7d\ ^1D_2$ state of barium

S. A. Bhatti, C. L. Cromer, and W. E. Cooke
Physics Department, University of Southern California, University Park, Los Angeles, California 90007
(Received 5 January 1981)

The $5d7d\ ^1D_2$ state of barium is configuration mixed with the $6snd$ Rydberg series. This work examines the large-r behavior of the Rydberg character of the mixed-state wave function by projecting it experimentally onto a series of known Rydberg states, $6P_{1/2}nd$, $J=3$. Results agree with calculations based on the quantum-defect characterization of the wave function. This work also presents an analytical approximation to the radial-wave-function overlap integral between Rydberg states of arbitrary energy.

I. INTRODUCTION

A recent analysis[1] of the $J=2$ states of barium using multichannel quantum-defect theory (MQDT) concludes that the "$5d7d$" state ($E=41\,841.5\ \mathrm{cm}^{-1}$) has 31% $5d7d$ character and 69% $6snd$ character. Thus, for a substantial fraction of time, the state behaves as a $6snd$ Rydberg state. According to MQDT, the large-radius (r) behavior of the nd Rydberg electron wave function should only depend on its binding energy relative to the $Ba^+(6s)$ ionization limit.[2] If an effective quantum number n^* is defined relative to the binding energy

$$W=-\frac{1}{2(n^*)^2}\ , \tag{1}$$

then for our state of interest $n^*=23.8$. For clarity, we will refer to the $6snd$ character of the $5d7d\ ^1D_2$ state as $6s23.8d$. This work examines the large-r behavior of the $6s23.8d$ state by projecting that state onto a series of unperturbed $6P_{1/2}nd$, $J=3$ states using isolated core excitation (ICE). The results are entirely consistent with the MQDT description.

Previous attempts to examine the Rydberg composition of perturbed states have measured characteristics which are not really dependent on the large-r behavior of the Rydberg wave function (e.g., magnetic g factors).[3] For unperturbed states, the situation is somewhat better. Polarizabilities,[4] Stark-field behavior,[5] and magnetic field behavior[6] have consistently shown agreement between calculations using simple, Coulombic, one-electron wave functions and measured quantities.

In the next section we will present calculations of the relative $5d7d \rightarrow 6P_{1/2}nd$ excitation strengths using the ICE model and discuss how these calculations are made using numerically integrated, one-electron wave functions based on quantum-defect theory. The third section will outline the experimental procedure and data reduction. The final section will discuss the comparison of theory and experiment.

II. THEORY

The isolated core excitation (ICE) technique utilizes atomic states which are composed of products of two very different one-electron wave functions.[7] With these states, the basic indistinguishability of electrons is removed insofar as it is easily possible to affect one wave function without perturbing the other. For a typical state, e.g., $6snd$, the two-product wave functions span entirely different regions of space, and therefore overlap (and any exchange effects) is only of the order $(n^*)^{-3}$. It thus becomes possible to excite only the "core" $6s$ electron with a laser, while the slow, Rydberg electron hardly responds at all. In our case, even though the $6s23.8d$ initial state is strongly configuration mixed with the $5d7d$, and the final $6pn'd$ state is mixed with continuum states like $Ba^+(5d)+e^-(\epsilon p)$, the transition moment will be dominated by the $6s23.8d \rightarrow 6pn'd$ term, rather than any terms due to direct photoionization.

However, the Rydberg electron is not entirely unperturbed by the core transition. The effect of the core on Rydberg wave function is usually treated using quantum-defect theory. The basic assumption of quantum-defect theory is that the Rydberg electron sees a pure Coulomb field outside some small core radius, r_c.[2] Under this assumption, the only effect of the core is to change the boundary condition on the wave function's phase at r_c from the hydrogenic value to some new value. The new value is determined by the requirement that the wave function inside the core (where a Coulomb solution is not valid) is zero at the origin. For $r>r_c$, the wave function is thus a specific combination of two independent solutions to the Coulomb potential such that it has the appropriate phase at $r=r_c$. Quantum-defect theory shows that if the required

phase at r_c is shifted from the hydrogenic value by $\pi\delta$, then only the solution with binding energy given by Eq. (1) for $n^* = n - \delta$ will be bound as $r \to \infty$. Multichannel quantum-defect theory shows that when several configurations interact, quantum-defect theory is still valid, but δ changes with n in a periodic fashion.

If the core is changed from $6s$ to $6p$, then it is entirely possible that the Rydberg electronic wave function may also change to have the appropriate phase at $r = r_c$, and thus the final state has a different quantum defect than the initial state, before the core excitation. Different quantum defects mean that the available Rydberg eigenstates have different energies, and thus different behavior, i.e., turning point and wave-function phase, in the large-r region. The net effect is that although the Rydberg electron originated in a well-defined, Rydberg state, it may be excited into any of a number of states depending on the energy of the photon absorbed by the core. The transition rate will depend on the overlap between the initial Rydberg state and the final $n'd$ Rydberg state. Thus, we will approximate for the transition dipole moment between a $6s23.8d$ state and a $6pn'd$ state:

$$\langle 6s23.8d|er|6pn'd\rangle = \langle 6s|er|6p\rangle\langle 23.8d|n'd\rangle , \qquad (2)$$

where the initial factor is the constant transition moment for the Ba^+ ion and the final overlap factor only depends on the binding energies of the $23.8d$ and $n'd$ Rydberg electrons, since most of the probability density for both $23.8d$ and $n'd$ states lie in the large-r region.

We have constructed one-electron Rydberg wave functions by a direct numerical integration of the radial differential equation for a Coulomb potential using a method similar to that of Zimmerman *et al.*[5] The integration begins at large values of r where the decaying asymptotic solution only depends on the binding energy and continues to small values of r, terminating when the wave function begins to show irregular behavior. Additionally, the variable r is scaled so that the change in r per step is small when the wave function changes rapidly and large when the wave function changes slowly.

Zimmerman *et al.*[5] used a logarithmic scaling of r; however, we wanted a variable scaling that would lead to sinusoidal, pseudo-free-particle solutions. Over much of the range of r, $v = \partial/\partial r \sim \sqrt{2/r}$, so that $\partial/\partial u \sim \sqrt{8}$ for $u = \sqrt{r}$. Thus, we have used a square-root scaling of r and a scaled wave function χ, which lead to the following replacement for the radial differential equation:

$$u = \sqrt{r} , \qquad (3a)$$

$$\chi = r^{3/4} R(r) , \qquad (3b)$$

$$\left[-\frac{\partial^2}{\partial u^2} + \left(\frac{2u}{n^*}\right)^2 - \frac{(2l+\frac{1}{2})(2l+\frac{3}{2})}{u^2} \right] \chi = 8\chi , \qquad (3c)$$

where $R(r)$ is the normal radial wave function and $n^* = n - \delta$ is the effective quantum number. Radial integrals are also scaled so that

$$\int_0^\infty R_{n_1} r^k R_{n_2} r^2 dr = \int_0^\infty \chi_{n_1} u^{2k} \chi_{n_2} u^2 du . \qquad (4)$$

Equation (3c) has simple, approximate solutions in the regions of large, intermediate, and small r:

$$\chi \sim u^{2n^*} e^{-(u/n^*)^2} , \quad r > n^{*2} \qquad (5a)$$

$$\chi \sim \sin(2\sqrt{2u} + \phi) , \quad (2l+1)^2 < r < (n^*)^2 \qquad (5b)$$

$$\chi \sim u^{1/2 \pm (2l+1)} , \quad r < (2l+1)^2 . \qquad (5c)$$

Note that in the intermediate range, where χ changes sign, a constant step size in u gives a constant number of steps per node. We used a Numerov integration method,[8] with a step size of 0.1 (approximately 10 steps per node). Figure 1 shows the numerically calculated wave functions

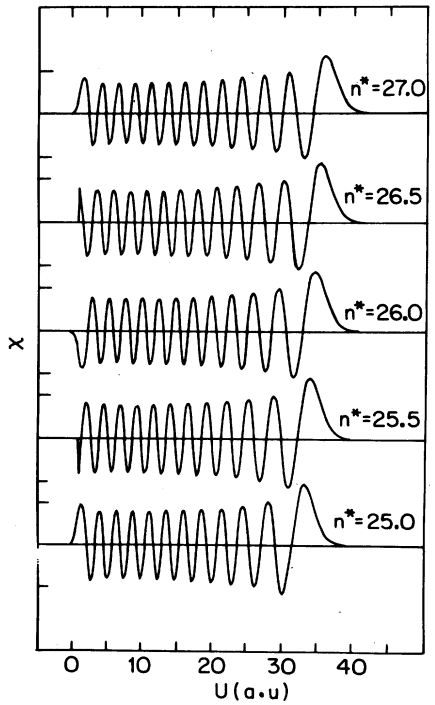

FIG. 1. Scaled radial wave functions $\chi(u) = r^{3/4} R(r)$ as a function of a scaled radius $u = \sqrt{r}$, for different effective quantum numbers between $n^* = 25$ and $n^* = 27$. Amplitude scale markers show ± 0.01 values. The wave-function sign was chosen so that the wave function would be positive for large u.

for n^* between 25 and 27. For integer n^*, the wave functions do converge to 0 at $u=0$, showing that relatively little phase error is accumulated during the integration procedure. Since we were only interested in overlap integrals [$k=0$ in Eq. (4)], we used the following approximation which is derived in the Appendix:

$$\int_0^\infty R_{n_1^*} R_{n_2^*} r^2 dr = (-1)^{n_2-n_1} \frac{2\sqrt{n_1^* n_2^*}}{n_1^*+n_2^*} \frac{\sin\pi(n_2^*-n_1^*)}{\pi(n_2^*-n_1^*)} . \quad (6)$$

III. EXPERIMENT

The Ba $5d7d\,^1D_2$ atoms were prepared by pulsed, stepwise excitation of atoms from an effusive atomic beam of Ba. The apparatus is described in detail elsewhere.[9] The initial excitation was in two steps: $6s^2 \rightarrow 6s6p\,^1P_1$ and $6s6p\,^1P_1 \rightarrow 5d7d\,^1D_2$ as shown in Fig. 2. Both lasers were right circularly polarized so that only the $m_J=+2$ state was populated. A third pulsed laser drove the final transition $5d7d\,^1D_2 \rightarrow 6P_{1/2}nd$, $J=3$, also shown in Fig. 2. It too was right-circularly polarized, so that only the $J=3$, $m_J=3$ states would be excited; this removed the possibility of ambiguity due to multiple J values for the $6pnd$ states (each of which could have a different width and energy). The $6P_{3/2}nd$ states were not involved since the $6P$ fine structure is ~380 Å, much larger than the scanning range of the third laser.

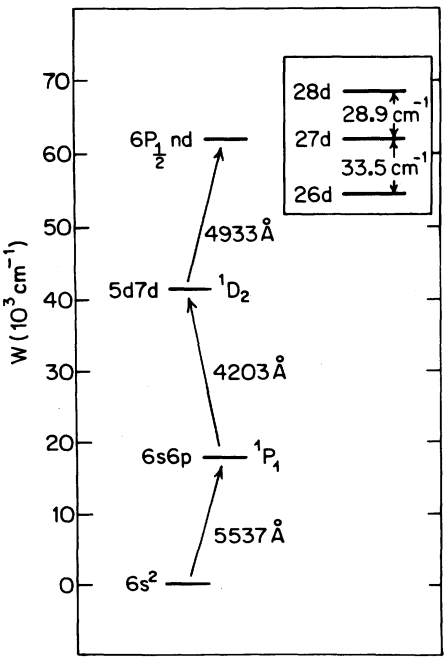

FIG. 2. Excitation diagram. Arrows represent laser excitations. The box shows the separation in cm^{-1} of some of the final $6P_{1/2}nd$ states.

Each of the $6P_{1/2}nd$ states autoionizes far more rapidly than their fluorescence rate, so that by collecting the total number of ions produced, we could determine the number of $5d7d$ atoms excited. As the wavelength of the third laser was scanned we obtained data as shown in Fig. 3. Where the multiple peaks represent the different $6P_{1/2}nd$, final states. The central region of Fig. 3 was taken at relatively low power so that the features would not be power broadened or saturated. The wings of Fig. 3 were taken at an increased power level so that the small features would be seen. The high- and low-power sweeps were combined by scaling according to the height of the first peak to the blue of the two major features. In Fig. 3, this scaling would lead to an amplification of the central region by a factor of 13.5. The narrow feature at 4948 Å is a wavelength marker due to resonant two-photon photoionization of Ba $6s6p\,^1P_1$ atoms as described in Ref. 7. The small central peak at 4935 Å was due to excitations from the $6s28s\,^1S_0$ state which was excited since the lasers were not perfectly polarized. (The $6s28s\,^1S_0$ state lies only 0.1 cm^{-1} below the "$5d7d$" state.[1])

The effective quantum number and autoionization linewidth Γ of each of the $6P_{1/2}nd$, $J=3$ states were determined independently by driving the transitions $6snd \rightarrow 6P_{1/2}nd$, $J=3$, which only have one major feature each. Figure 4 shows a plot of quantum defect and $\Gamma(n^*)^3$ (a.u.) for $n=23$ to 33. The large uncertainty on Γ results primarily

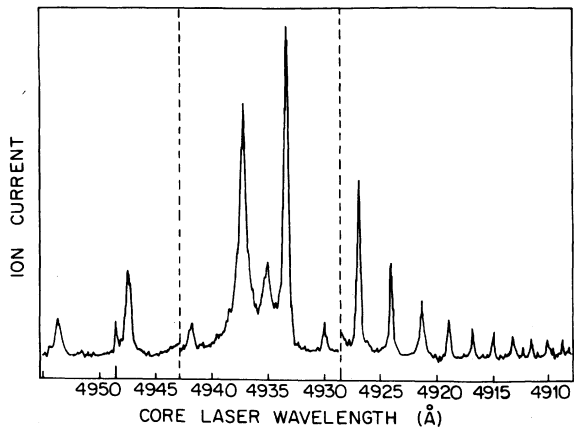

FIG. 3. Excitation spectrum for the $5d7d\,^1D_2 \rightarrow 6P_{1/2}nd$, $J=3$ transitions. For the center region, between the dashed lines, the laser power was reduced by a factor of 13.5 to avoid power broadening of those transitions. The different peaks represent different n values for the final state. The feature at 4948 Å is a laser-frequency marker. The feature at 4935 Å is due to the $6s28s \rightarrow 6P_{1/2}28s$ transition due to imperfect preparation of the $5d7d$ state.

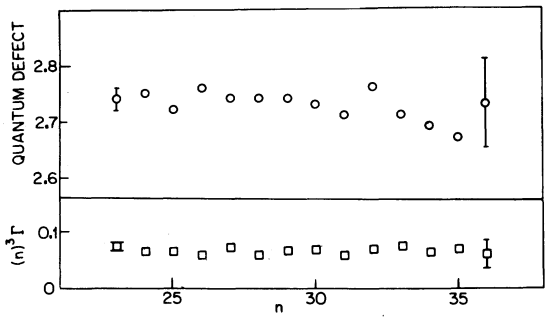

FIG. 4. Quantum defects and autoionization broadened linewidths of the $6P_{1/2}nd$, $J=3$ states.

from our third laser linewidth (0.4 ± 0.1 cm^{-1}), which was substantial when compared to the total linewidth of the highest states (0.9 cm^{-1}).

IV. ANALYSIS AND DISCUSSION

In order to compare the calculated and measured excitation efficiencies to each $6P_{1/2}nd$ state, it is important to determine the total area under each of the peaks in Fig. 3. However, the background level and the uncertainty in feature width make this very difficult. As an alternative we have instead measured the baseline-to-peak amplitudes and multiplied by $(n^*)^{-3}$ since, as Fig. 4 shows, the widths of the $6P_{1/2}nd$ states scale as $(n^*)^{-3}$. Since the peaks were generally symmetric, we expect less than 20% error to result from the procedure. The peak positions were similarly determined from the quantum-defect measurements shown in Fig. 4, although there was very little difference between those and a direct reading of position from Fig. 3.

The comparison between measurement and calculation is shown in Fig. 5, where the data points, represented by "X" are plotted along with the calculated values of the square of the overlap between the 23.8d state and representative states with n^* in the range 20–34. As noted earlier, the overall normalization factor is arbitrary and only the relative variation is determined. The good agreement over $2\frac{1}{2}$ orders of magnitude demonstrates the validity both of the quantum-defect wave functions and of the ICE model.

It should be emphasized, however, that the quantum-defect wave functions are only valid in regions of large r. In regions of small r, the true wave function is a complex combination of $5d7d$ character and $6snd$ character, where neither portion is well described by simple one-electron wave functions. This means, of course, that the projection defined in Eq. (2) will only be valid for highly excited states $n \gg 1$, which encompass only a small energy regime.

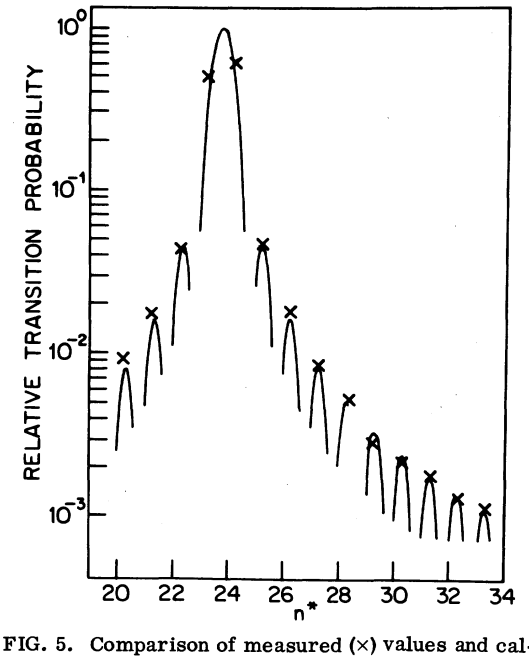

FIG. 5. Comparison of measured (×) values and calculated values (solid line) for the relative transition probability from a $6s$ 23.8d to $6P_{1/2}n^*d$ states for different values of n^*. The solid line is given by Eq. (6) in the text.

ACKNOWLEDGMENTS

This work was supported by the National Science Foundation under Grant No. PHY78-16444. Some of the equipment used was provided by the Research Corporation. We would like to thank John Nodvik for suggesting the integration method used in the Appendix.

APPENDIX

To calculate properties of the Rydberg wave functions that do not depend on their behavior near the origin (which includes matrix elements of r^k for $k \geq 0$), we may ignore the centripetal terms and use the simpler equation:

$$-\frac{\partial^2}{\partial u^2}\chi + \left(\frac{2u}{n^*}\right)^2 \chi \equiv H_{n^*}\chi = 8\chi \ . \tag{A1}$$

Matrix elements calculated with this χ will typically result in errors of the order $(n^*)^{-3}$. However, for nonhydrogenic systems where an additional, unknown core potential is involved, such an error would be present anyway. The solution of Eq. (A1), which asymptotically goes to 0 for large u, is the parabolic cylinder function $U(-2n^*, 2u/\sqrt{n^*})$.[10]

Overlap integrals can be performed exactly with these functions. Note that

$$\chi_{n_2} H_{n_1} \chi_{n_1} - \chi_{n_1} H_{n_2} \chi_{n_2} = 0 \tag{A2}$$

since the different solutions have the same effective energy, 8, but different effective potentials, $(2u/n^*)^2$. Thus

$$4\left(\frac{1}{n_1^{*2}}-\frac{1}{n_2^{*2}}\right)\int_0^\infty \chi_{n_2}\chi_{n_1}u^2du = \int_0^\infty \chi_{n_2}\frac{\partial^2}{\partial u^2}\chi_{n_1} - \chi_{n_1}\frac{\partial^2}{\partial u^2}\chi_{n_2}du \quad \text{(A3a)}$$

$$= \chi_{n_2}\chi'_{n_1} - \chi_{n_1}\chi'_{n_2}\Big|_0^\infty . \quad \text{(A3b)}$$

Now, using the values of a normalized parabolic cylinder function and its derivative at $u=0$, we obtain

$$\int \chi_{n_2}\chi_{n_1}u^2du = \frac{4\sqrt{n_1^*n_2^*}}{n_1^*+n_2^*}\frac{1}{\pi(n_2^*-n_1^*)} \times\left[\left(x-\frac{1}{x}\right)\cos\pi(n_2^*+n_1^*) + \left(x+\frac{1}{x}\right)\sin\pi(n_2^*-n_1^*)\right], \quad \text{(A4)}$$

where x is defined

$$x^2 = \frac{\Gamma(n_2^*+\frac{1}{4})}{\Gamma(n_1^*+\frac{1}{4})}\frac{\Gamma(n_1^*+\frac{3}{4})}{\Gamma(n_2^*+\frac{3}{4})} . \quad \text{(A5)}$$

For $|(n_2^*-n_1^*)| \ll n_1^*$, x is very close to 1. If we let $x=1$ and introduce a phase factor so that both wave functions have the same sign at the origin, Eq. (6) results. Equation (6) was checked against numerical integration for overlaps between $n_1^*=23.8$ and $n_2^*=20$ to 34. Typically, the two methods agreed to better than 0.5%. For $n_2^*-n_1^*$ equal to an integer +0.1, the difference was as large as 1%, but the overlaps themselves were small, since this is near the orthogonality condition.

It should be noted that the same results would be obtained if the integration is begun at some small value $r_c>0$. For small u, the parabolic cylinder function behaves as $\sin(\sqrt{8u}+\phi_{n^*})$, so that Eq. (A3b) becomes $\sin(\phi_{n_1^*}-\phi_{n_2^*})$, independent of the choice of origin.

[1]M. Aymar and O. Robaux, J. Phys. B 12, 531 (1979).
[2]K. T. Lu and U. Fano, Phys. Rev. A 2, 81 (1970).
[3]J. J. Wynne, J. A. Armstrong, and P. Esherick, Phys. Rev. Lett. 39, 1520 (1977).
[4]T. F. Gallagher and W. E. Cooke, Phys. Rev. A 18, 2510 (1978).
[5]M. L. Zimmerman, M. G. Littman, M. M. Kash, and D. Kleppner, Phys. Rev. A 20, 2251 (1979).
[6]M. L. Zimmerman, J. C. Castro, and D. Kleppner, Phys. Rev. Lett. 40, 1083 (1978).
[7]W. E. Cooke and T. F. Gallagher, Phys. Rev. Lett. 41, 1648 (1978).
[8]J. M. Blatt, J. Comput. Phys. 1, 382 (1967).
[9]W. E. Cooke, S. A. Bhatti, C. L. Cromer, T. F. Gallagher, K. A. Safinya, and W. D. Sandner, unpublished.
[10]M. Abramowitz and I. Stegun, *Handbook of Mathematical Functions* (Dover, New York, 1970), p. 687.